COMBINED LOADING FRACTURE TRAJECTORIES OF VISCOELASTIC MATERIALS

Stephen Alfred Marinshaw

NAVAL POSTGRADUATE SCHOOL
Monterey, California

THESIS

COMBINED LOADING FRACTURE TRAJECTORIES
OF
VISCOELASTIC MATERIALS

by

Stephen Alfred Marinshaw, Jr.

Thesis Advisor: G. H. Lindsey

June 1973

Approved for public release; distribution unlimited.

Combined Loading Fracture Trajectories of Viscoelastic Materials

by

Stephen Alfred Marinshaw, Jr.
Lieutenant, United States Navy
B.S., University of Maryland, 1963

Submitted in partial fulfillment of the
requirements for the degree of

AERONAUTICAL ENGINEER

from the

NAVAL POSTGRADUATE SCHOOL
June 1973

ABSTRACT

The critical stress intensity factors and fracture trajectories for both filled and unfilled viscoelastic plane stress specimens were experimentally determined by controlled crack elongation. Fracture testing included combined displacement loadings both of single and bi-material specimens with initial cracks located in each material and at the bi-material interface.

The feasibility of trajectory prediction using an elastic linear-strain finite-element analysis was investigated. Techniques for adapting the elastic model grid patterns to predict viscoelastic trajectories were developed.

Measured trajectories correlated well with the directions of maximum principal stress as determined by the finite-element solution of a blunt crack-tip model.

TABLE OF CONTENTS

LIST OF FIGURES

ACKNOWLEDGEMENTS

The author wishes to express his gratitude to United Technology Center, Sunnyvale, California, for providing the laboratory facilities and test materials used in this study. He is especially grateful to Mr. E. C. Francis and Dr. L. I. Deverall of United Technology Center for their support and technical assistance.

The author also wishes to thank Professor Gilles Cantin of the Naval Postgraduate School for assistance with the finite-element studies and Professor Gerald H. Lindsey for his supervision and constant encouragements throughout.

I. INTRODUCTION

A. BACKGROUND

During the manufacture of solid propellant rocket motors, it is possible for stresses to develop during cure cooldown of sufficient magnitude to induce fracture at physical discontinuities and internal flaws. Such cracks may be tolerable providing the trajectories do not create significant additional burning surface nor expose the case to combustion temperatures by local failure of the insulation. The direction of crack propagation is therefore of considerable significance. The stress levels for fracture propagation are of equal interest. It is therefore desirable to study the behavior of these viscoelastic materials and to develop techniques for evaluating their critical fracture criteria.

The fracture stresses are commonly expressed in terms of the stress intensity factors K_I, K_{II} and K_{III} where the subscript refers to the fracture mode as shown in Figure 1.

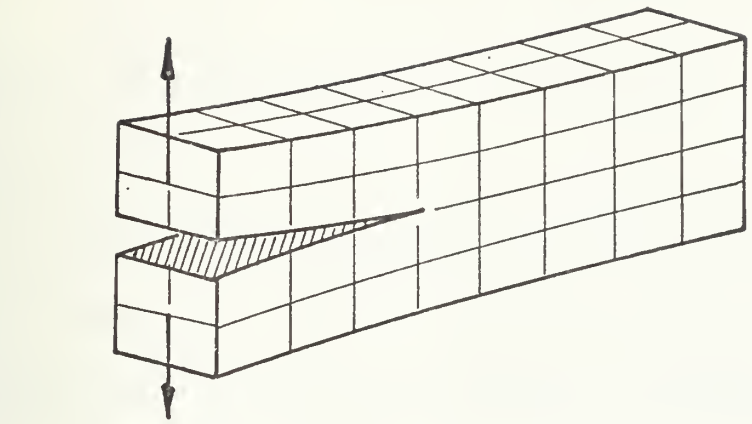

K_I

Mode I
(Opening Mode)

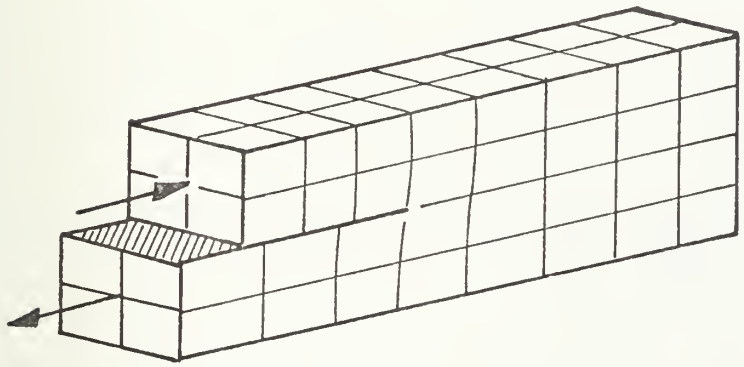

K_{II}

Mode II
(Shearing Mode)

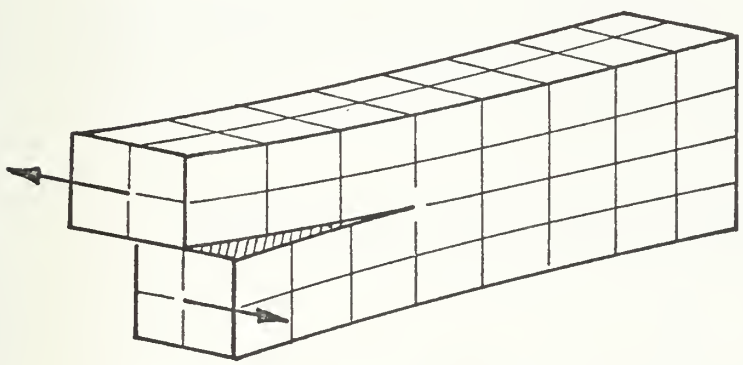

K_{III}

Mode III
(Tearing Mode)

Figure 1. Fracture Modes.

B. CLASSICAL SOLUTION

The study of fracture mechanics, to a large extent, has dealt primarily with the opening mode behavior of elastic materials.

The classical solution to the detailed stress field of a sharp-tipped crack as shown in Figure 2 was formulated by Williams and given by Sih and Liebowitz [1] as:

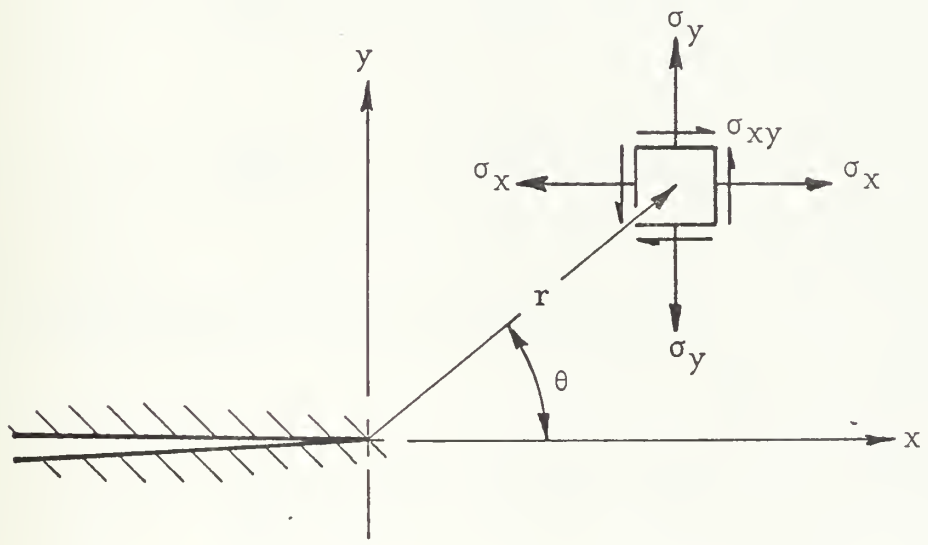

Figure 2. Stress Field Coordinate System.

Symmetric Case (Mode I)

$$\sigma_x = \frac{K_I}{\sqrt{2r}} \cos\frac{\theta}{2}\left[1 - \sin\frac{\theta}{2}\cdot\sin\frac{3\theta}{2}\right] + \ldots \quad (1a)$$

$$\sigma_y = \frac{K_I}{\sqrt{2r}} \cos\frac{\theta}{2}\left[1 + \sin\frac{\theta}{2}\cdot\sin\frac{3\theta}{2}\right] + \ldots \quad (1b)$$

$$\sigma_{xy} = \frac{K_I}{\sqrt{2r}} \cos\frac{\theta}{2}\left[\sin\frac{\theta}{2}\cdot\cos\frac{3\theta}{2}\right] + \ldots \quad (1c)$$

and

$$u = \frac{K_I\sqrt{2r}}{8G}\left[(2\kappa-1)\cos\frac{\theta}{2} - \cos\frac{3\theta}{2}\right] + \ldots \quad (2a)$$

$$v = \frac{K_I\sqrt{2r}}{8G}\left[(2\kappa+1)\sin\frac{\theta}{2} - \sin\frac{3\theta}{2}\right] + \ldots \quad (2b)$$

Skew-Symmetric Case (Mode II)

$$\sigma_x = \frac{-K_{II}}{\sqrt{2r}} \sin\frac{\theta}{2}\left[2 + \cos\frac{\theta}{2}\cdot\cos\frac{3\theta}{2}\right] + \ldots \quad (3a)$$

$$\sigma_y = \frac{K_{II}}{\sqrt{2r}} \sin\frac{\theta}{2}\left[\cos\frac{\theta}{2}\cdot\cos\frac{3\theta}{2}\right] + \ldots \quad (3b)$$

$$\sigma_{xy} = \frac{K_{II}}{\sqrt{2r}} \cos\frac{\theta}{2}\left[1 - \sin\frac{\theta}{2}\cdot\sin\frac{3\theta}{2}\right] + \ldots \quad (3c)$$

and

$$u = \frac{K_{II}\sqrt{2r}}{8G}\left[(2\kappa+3)\sin\frac{\theta}{2} + \sin\frac{3\theta}{2}\right] + \ldots \qquad (4a)$$

$$v = \frac{K_{II}\sqrt{2r}}{-8G}\left[(2\kappa-3)\cos\frac{\theta}{2} + \cos\frac{3\theta}{2}\right] + \ldots \qquad (4b)$$

where $\kappa = 3 - 4\nu$ Plane Strain

$$\kappa = \frac{3 - \nu}{1 + \nu}$$ Plane Stress

George Irwin related the stress intensity factor to the strain energy release rate by computing the work done at a propagating crack tip. His results for K_I show that:

$$K_I^2 = \frac{-E}{\pi t}\frac{dU}{dc} \qquad (5)$$

By means of the energy balance introduced by A. A. Griffith in the early 1920's, it can be shown that K_{IC}, the value of K_I at fracture, must be a material property.

C. COMBINED LOADING

Previous studies [2] concerning stress fields in rocket motor castings indicate approximately equal shear and tension at the propellant-liner interface near the motor end surfaces. It is therefore desirable to investigate the behavior of such materials under a combined loading condition.

Adaptation of the classical solutions for single-mode stress fields to the combined-mode case requires only superposition of the respective solutions. Combining the opening and shearing modes, we then have:

$$\sigma_x = \frac{1}{\sqrt{2r}}\cos\frac{\theta}{2}\{K_I[1-\sin\frac{\theta}{2}\cdot\sin\frac{3\theta}{2}]-K_{II}\tan\frac{\theta}{2}[2+\cos\frac{\theta}{2}\cdot\cos\frac{3\theta}{2}]\} \quad (6a)$$

$$\sigma_y = \frac{1}{\sqrt{2r}}\cos\frac{\theta}{2}\{K_I[1+\sin\frac{\theta}{2}\cdot\sin\frac{3\theta}{2}]+K_{II}\tan\frac{\theta}{2}[\cos\frac{\theta}{2}\cdot\cos\frac{3\theta}{2}]\} \quad (6b)$$

$$\sigma_{xy} = \frac{1}{\sqrt{2r}}\cos\frac{\theta}{2}\{K_I[\sin\frac{\theta}{2}\cdot\cos\frac{3\theta}{2}]+K_{II}[1-\sin\frac{\theta}{2}\cdot\sin\frac{3\theta}{2}]\} \quad (6c)$$

In polar coordinates, the stresses are given as:

$$\sigma_r = \frac{1}{2\sqrt{2r}}\cos\frac{\theta}{2}[(3-\cos\theta)K_I + (3\cos\theta-1)K_{II}\tan\frac{\theta}{2}] + \ldots \quad (7a)$$

$$\sigma_\theta = \frac{1}{2\sqrt{2r}}\cos\frac{\theta}{2}[(1+\cos\theta)K_I - 3K_{II}\sin\theta] + \ldots \quad (7b)$$

$$\tau_{r\theta} = \frac{1}{2\sqrt{2r}}\cos\frac{\theta}{2}[K_I\sin\theta + K_{II}(3\cos\theta-1)] + \ldots \quad (7c)$$

It can be seen that the general formulation of the combined loading solution may be expressed as:

$$\sigma = f(r)\cdot g(\theta, K_I, K_{II}) \quad (8)$$

Two commonly recognized hypotheses for crack extension in a brittle (non-viscoelastic) material under slowly applied loads are:

a) The crack extension starts at its tip in the radial direction, and

b) The crack extension starts in the plane perpendicular to the direction of greatest tension.

These state that a crack will extend radially in the direction of maximum tangential stress where the shear stress is zero. Consistent with the theory of Griffith, the direction of crack propagation corresponds to the direction of maximum energy release. This direction has been

identified as the maximum principal stress direction.

It is intended herein to demonstrate that the fracture trajectories of viscoelastic materials may be predicted by the maximum principal stress directions as determined by elastic analyses. To minimize the time-dependent viscoelastic effects, the loads were slowly applied in order to approximate an "equilibrium" condition.

In order to determine the direction of maximum principal stress, the detailed stress field in the vicinity of the crack tip must be known. Williams' solution, based on an infinite sheet with a sharp-tipped central crack, has generally been accepted for any geometry in the "vicinity" of the crack tip. Definition of this "vicinity" varies with sample geometry. Another method of establishing the stress field is by finite-element techniques.

There are two basic objectives of this study: 1) to demonstrate that the linear-strain finite-element solution is suitable for fracture analyses by correlation with the classical field for a sharp-tipped crack, and 2) to apply the finite-element technique to determine the direction of maximum principal stress for the blunt-tipped crack geometry, which models the viscoelastic materials at fracture.

The results of crack elongation tests under combined loading with constant boundary displacements have been correlated herein with the trajectory predictions made by finite-element methods.

II. EXPERIMENTAL STUDIES

A series of combined loading tests was performed on selected material specimens. The geometry of the specimens, whose fracture behavior is independent of crack length, is shown in Figure 3. An initial crack length of 1.0 inch was chosen for all tests.

A. DESCRIPTION OF SAMPLES

Three basic specimens of the same geometry but different material properties were examined in this study: 1) an unfilled viscoelastic liner material, 2) a filled viscoelastic propellant sample, and 3) a composite specimen which models the propellant-liner interface. Initial cracks were made both along the centerline and offset 0.2-inches from the centerline. The specimens were subjected to combined loading by constant boundary displacements ranging from pure opening (Mode I) to pure shear (Mode II).

B. SAMPLE FABRICATION

The samples were fabricated by United Technology Center, Sunnyvale, California. The propellant and/or liner materials were cast in redwood boxes. The wood, which was

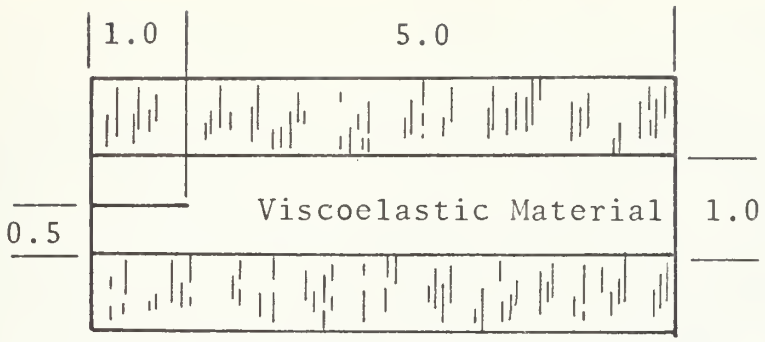

a. Single Material (Centerline Crack)

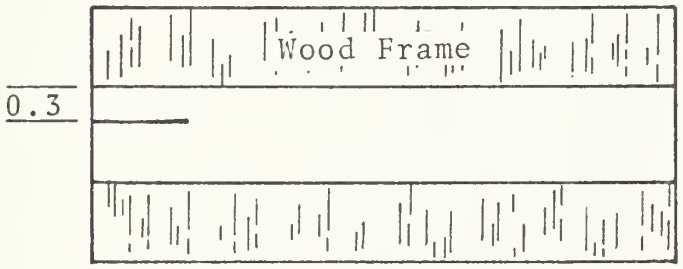

b. Single Material (Offest Crack)

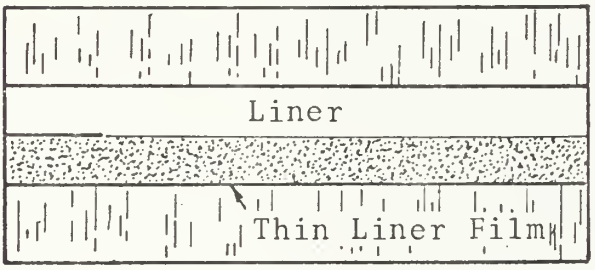

c. Bi-Material (Centerline Crack)

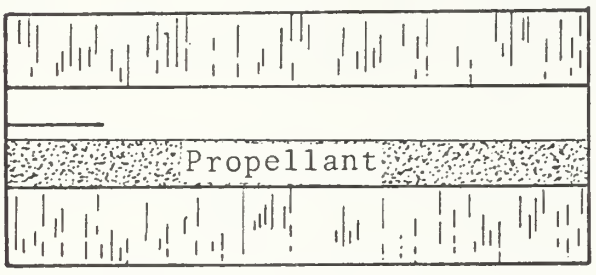

d. Bi-Material (Offset Crack)

Figure 3. Geometry of Test Specimens.

easily cut and shaped to the desired geometry, provided a semi-rigid boundary to the rubbery materials for installation in the testing apparatus. The inner surfaces of the wood were coated with an epoxy cement which penetrated the wood and provided a bonding agent for the liner. Since the propellant does not adhere to the epoxy or to the wood, a thin film of liner (to which the propellant bonds well) was applied to the epoxy permeated surfaces. The samples were cured in the boxes and later sawed and milled into 0.10-inch thick specimens.

The propellant samples were determined to be relatively uniform but the liner samples possessed a "soft" region extending from the wood boundaries approximately 0.15-inches into the sample itself, resulting from incomplete cure near the extremities. The region was identified by a tacky surface with a glossy appearance. This undesirable feature resulted in severe necking, which precluded accurate determination of strain levels during testing. The effective gage length was reduced from the specimen height of 1.0 inch to a maximum of 0.7 inch for the single-material specimens and to a maximum of 0.35 inch for the composite samples (on the liner half). The resultant force along the

direction of displacement was measured and modulus data were obtained from separate tests of the biaxial specimens.

C. SAMPLE PREPARATION FOR FRACTURE TESTING

The initial cracks were made by cutting a one-inch slit in the samples with a knife. The crack tip location was marked by grid lines drawn on the sample itself with a fine point drawing pen (No. 00 Rapidograph). The grid lines facilitated detection of crack propagation and were used to determine the strain in modulus evaluation tests. The displacements of the grid nodes were optically measured with a cathetometer, since the "soft" areas invalidated cross-head travel data as a method of strain determination. Mechanical testing indicated the moduli varied by as much as 50-percent between batches, and an equal variation within the same batch could be expected for different configurations and/or material aging time between tests. (The propellant is extremely hygroscopic. During initial tests the samples were retained in a dry nitrogen atmosphere, but due to the unavailability of a controlled environment during tests at NPS, the samples were allowed to age unrestrained. This affected the critical load levels, but the trajectories are independent of absolute moduli).

D. LABORATORY PROCEDURES

1. Description of Hardware

The combined-loading tests required construction of a specimen-holding apparatus, shown in Figure 4, which would allow rigid-body displacements of the specimen boundaries ranging from $\gamma = 0°$ to $\gamma = 90°$.

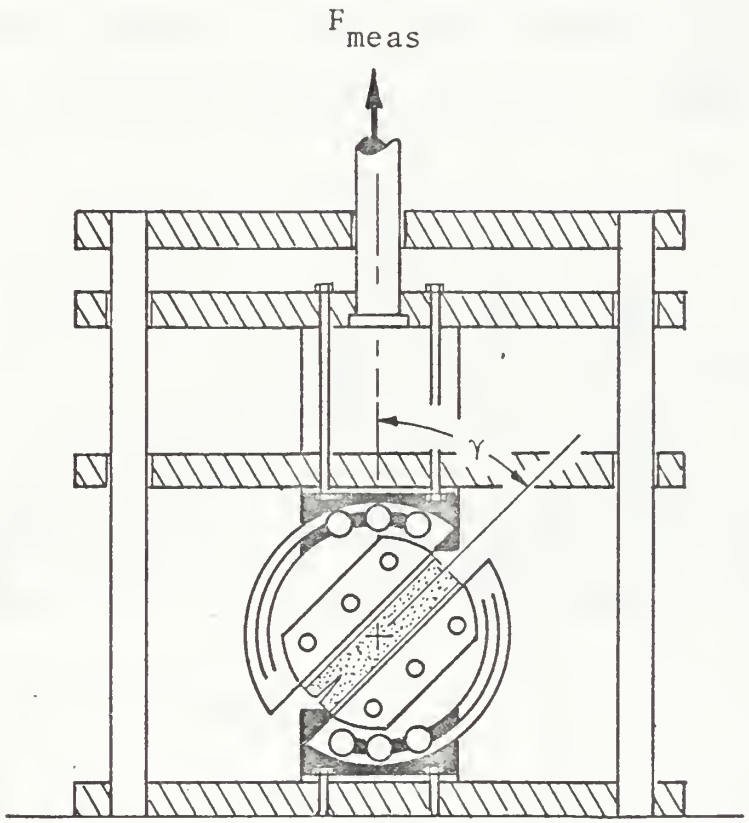

Figure 4. Drawing of Specimen Loading Fixture.

2. Force Measurement Under Combined Loading

Using the finite-element solution for stress distribution along the constant-displacement boundaries, the loading condition of a sample was determined by measuring the force component in the direction of displacement. This force was transmitted to the testing machine load cell, and recorded, to establish the stress intensity factors. By measuring the applied load vs. displacements, the influence of the "soft" regions at the liner-to-wood interface was minimized. The loading diagram is shown in Figure 5.

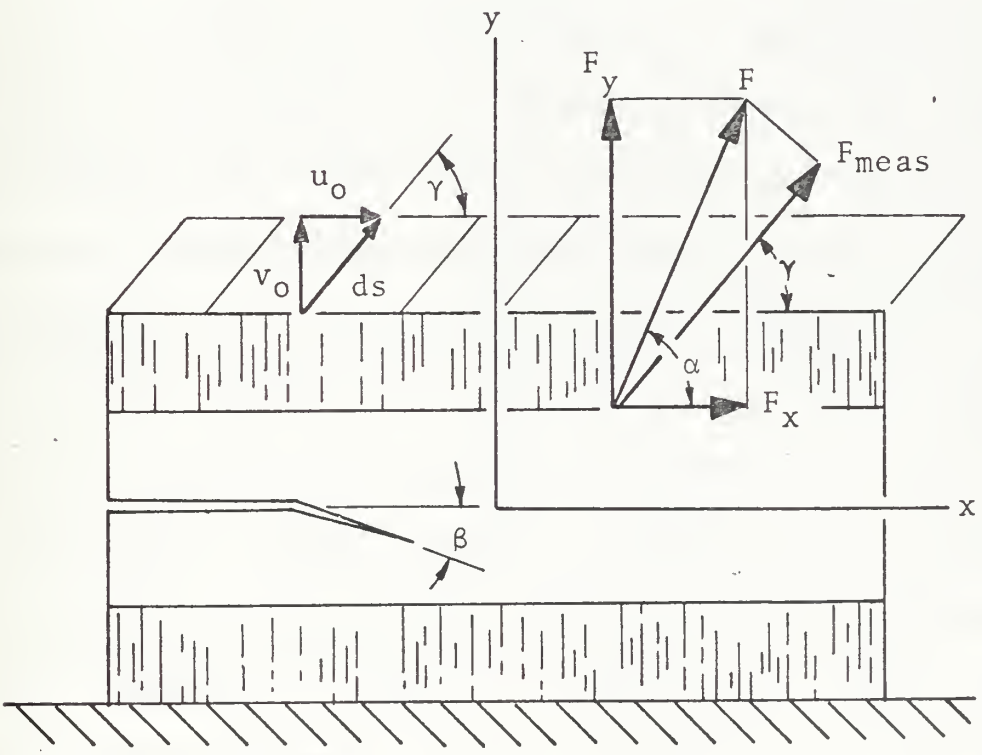

Figure 5. Loading Diagram of Material Sample.

3. Detection of Crack Elongation

Identification of fracture loads was hindered by the extreme low crack propagation velocities associated with viscoelastic fracture at low loading rates. During all fracture tests the loading rate was maintained at 0.05 inch per minute. Three techniques were employed, each of which provided limited success in critical load identification:

a. Separation of Grid Lines

The method most frequently used consisted of 5X optical observation of the crack-tip grid lines. With a high-intensity lamp illuminating the crack-tip area, it was possible to determine when the crack penetrated the vertical line located at the crack tip as shown in Figure 6. This method worked equally well with both liner and propellant. In general, the crack propagation was easier to detect in the propellant samples because elongation was erratic, sharp-tipped, and the material surface highly reflective, thereby enhancing optical techniques. The liner deformations at fracture levels maintained an elliptical crack-tip geometry.

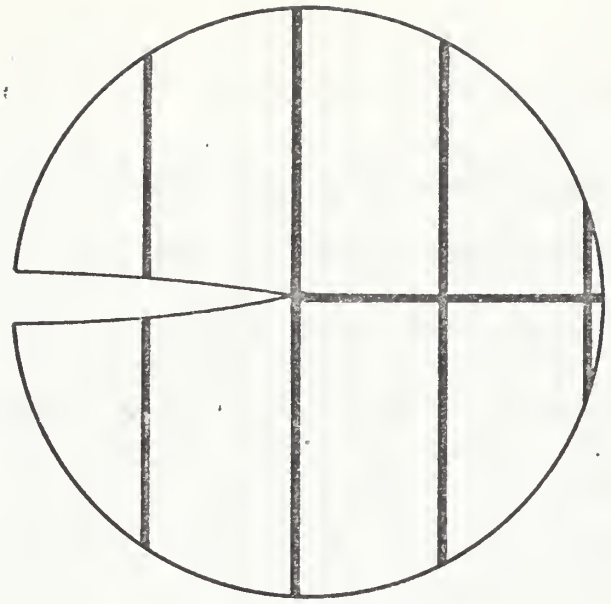

a. Grid Lines Prior to Crack Elongation.

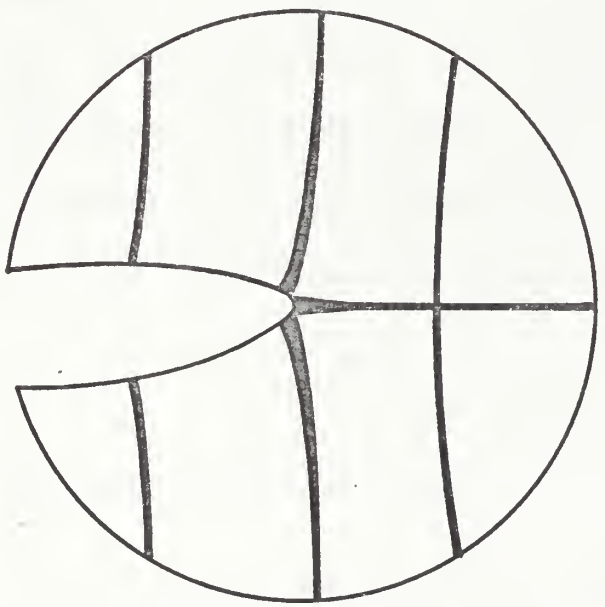

b. Separated Grid Line at Critical Load.

Figure 6. Crack Propagation Grid Lines.

b. Optical Observation of Crack Surface

An alternate optical technique was used with the liner samples when the boundary displacement angles were greater than 45°. Pre-fracture deformation opened the initial cracks approximately 0.2 inch. The surfaces were painted with drawing ink when the opening reached approximately 0.1 inch. The high intensity light was aimed along the crack line at the internal crack tip. The ink dried quickly and the crack elongation was identified by parting of the blackened fracture surface. A 5X eyepiece was also used with this technique, but the phenomenon could quite well be observed by the naked eye. This technique did not work with the propellant since pre-fracture strains did not sufficiently open the crack to allow preparation and observation.

c. Fluctuation of Load Data

A third technique was quite successful with propellant samples due to their erratic crack-elongation behavior. The data acquisition system was adjusted to maximum gain with zero offset so that recorded data emcompassed only a narrow band of force level. (Typical

fracture loads were in the order of 15 pounds. Amplification to produce 5 pounds full-scale recorder deflection with a 10-pound zero offset was used.) Tension up to the critical load produced a smooth data trace. Propagation of the crack was easily detected by fluctuations of the data trace. (Friction of the loading device typically produced load data-trace perturbations in the order of 0.05 pound peak-to-peak (PTP) or 0.10 inch during pre-fracture loading. The propellant samples' erratic crack propagation produced fluctuations in the order of 0.20 pound PTP or 0.40 inch on the recorded trace.) This technique correlated well with the optical method of grid line separation.

4. Trajectory Measurement

The trajectories were optically determined following specimen removal from the test rig, and relaxation to original shape. The liner fracture was characterized by a well-defined straight trajectory. The propellant trajectories were not smooth, but zig-zagged about a rather well-defined constant-direction path. Samples of each are shown in Figures 7 and 8.

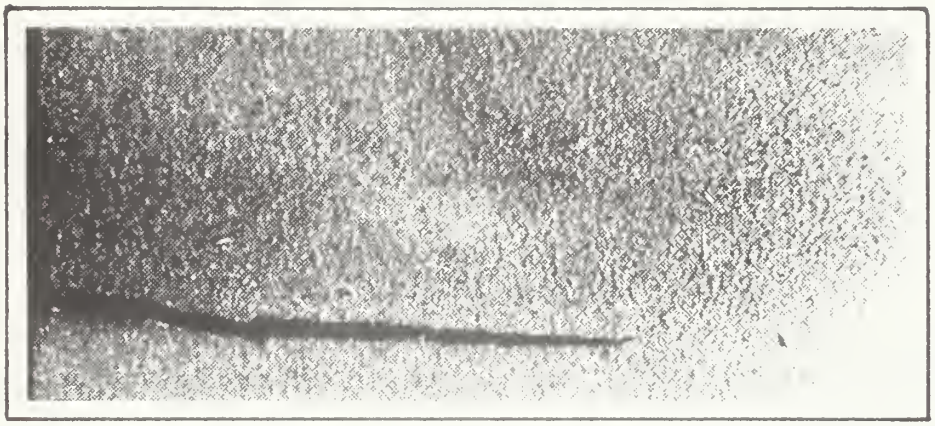

Figure 7. Photograph of Fracture in Liner Material.

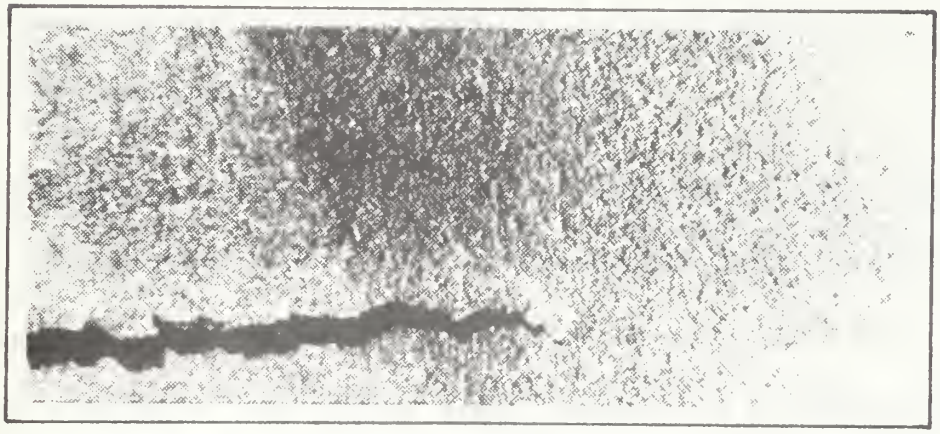

Figure 8. Photograph of Fracture in Propellant.

IV. COMPUTER METHODS

A. FINITE-ELEMENT SOLUTION

1. General Description of PSELST

The analytical solution for the elastic model of the labratory tests was generated by the finite element method. The basic program, PSELST (Plane Stress Elastic Analysis using Linear Strain Triangles) was written by Dr. Carlos A. Felippa [3] at the University of California (Berkeley, June 1966) and reprogrammed to allow initial displacement boundary conditions by J. P. Malone [4] at the Naval Postgraduate School in July 1968.

Displacement-compatible finite elements are used to ensure convergence. PSELST computes in-plane deflections and stresses at selected sites on the body resulting from in-plane loading. The basic mesh element is a quadrilateral composed of four 6-nodal-point linear strain triangles, the center point being the centroid (Figure 9).

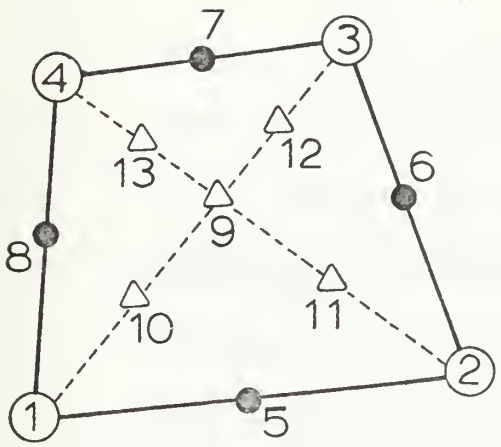

Quadrilateral

(4 Corner Nodes, 8 External Nodes)
(#9 = Centroid)

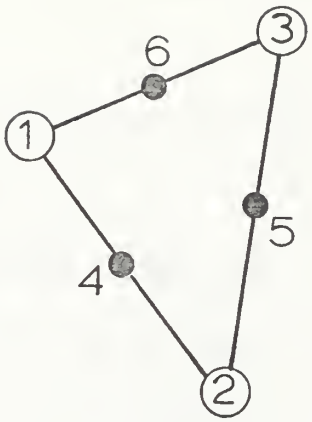

Triangle

(3 Corner Nodes,
6 External Nodes)

Figure 9. Linear-Strain Triangles of Basic Mesh Elements.

A detailed description of the program may be found in Reference 4.

2. Grid Mesh Design

Generation of the finite-element grid mesh is the single most important (and time-consuming) aspect of this solution method. While certain ground rules are established for efficient grid design, selection of an optimum pattern, if such exists, requires considerable trial and error. In

this study twelve patterns were examined which were essentially element-size variations of four basic designs:

1) Rectangular elements.
2) Rectangular elements with triangular elements in the vicinity of the crack tip.
3) Quadrilateral elements with polar symmetry and triangular elements at the crack tip.
4) Quadrilateral elements with polar symmetry and finite radius at the crack tip.

Schematics of each are shown in Figure 10.

B. CALCULATION OF INTERNAL STRAIN ENERGY

The internal strain energy may be computed by integration of the element stresses or displacements or, in the case of a conservative system, by computing the work at the structure boundaries. The latter technique requires considerably less effort, and since boundary stresses and displacements were provided by PSELST, a numerical integration program using Simpson's method was employed to compute the strain energy. The change in strain energy resulting from crack elongation was computed by repeating the entire solution process with an extended initial crack under identical loading conditions.

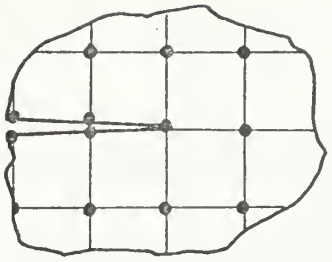

a. Rectangular Elements

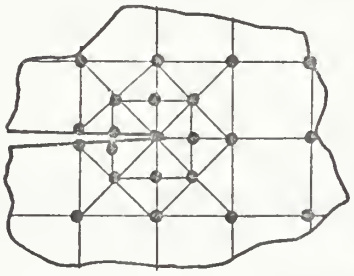

b. Rectangular Elements with Triangles at Crack Tip

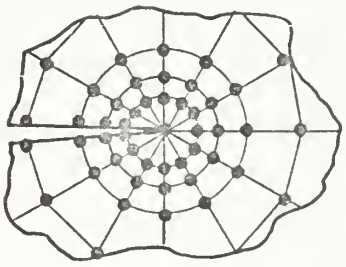

c. Polar Quadrilaterals with Triangles at Crack Tip

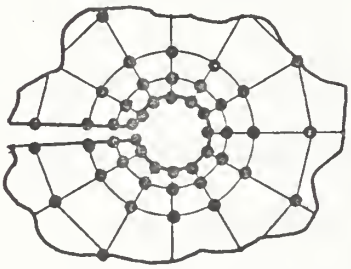

d. Polar Quadrilaterals with Finite Crack Tip Radius

Figure 10. Mesh Grid Patterns at Crack Tip.

IV. ANALYSIS AND RESULTS

A. EVAIUATION OF FINITE-ELEMENT METHOD

Evaluation of the finite-element method as a solution technique consisted essentially of validating the solution in two basic areas:

1. General Behavior of the Solution

Similar to the stress solutions, the displacement fields of Williams are a product solution; that is,

$$u = f_1(r) \cdot g_1(\theta) \tag{9a}$$

$$v = f_2(r) \cdot g_2(\theta) \tag{9b}$$

where $f(r)$ and $g(\theta)$ are given in Equations (2) and (4). We may check the r and θ behavior independently by plotting the computer solutions in the vicinity of the crack tip at constant θ or r. If agreement with the classical solution exists, this process also establishes the bounds of validity for the classical solution as represented by the singular

term of the series. A typical set of displacement curves for (v) at θ = constant is presented in Figure 11. Similar results were obtained for the displacements (u). This shows excellent correlation for a one-inch crack within a radius of 0.004 to 0.100 inch from the crack tip for the gecmetry shown. A representation of the θ-dependence for a boundary displacement angle of $\gamma = 37.5^{o}$ is shown in Figure 12. This also correlates well with the classical solution. The data shown in these figures represent solutions from the grid pattern of Figure 10c (polar quadrilaterals with triangles at crack tip). This pattern produced the best solution agreement with the classical in the vicinity of the crack tip. Determining the optimum grid pattern was essentially a task of evaluating the solution convergence to classical r and θ behavior.

2. Evaluation of Stress Intensity Factors

a. Simultaneous Solution of Classical Equations

A correct solution requires K_I and K_{II} to be constants for any given loading of the fixed geometry. It is therefore possible to solve for these quantities by simultaneous solution of two linear algebraic equations

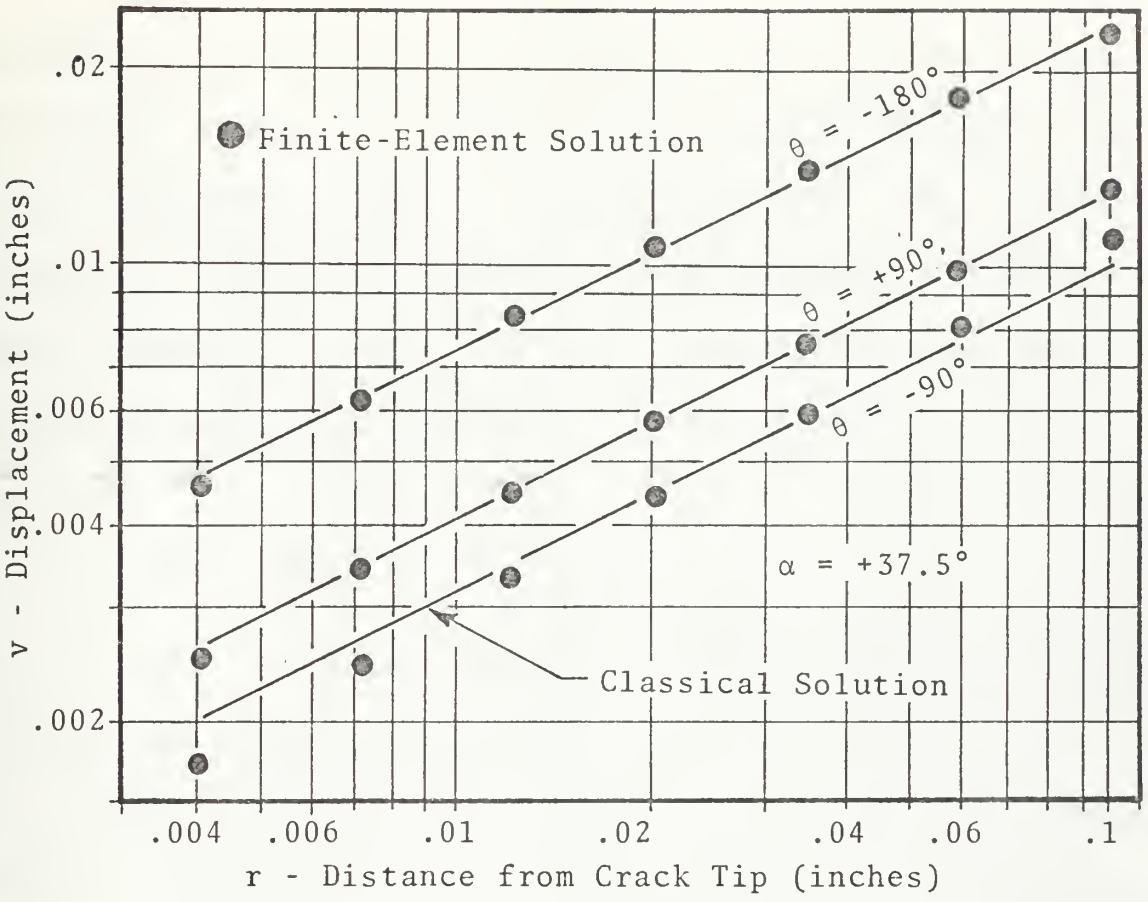

Figure 11. Typical Displacement Curves at θ = Constant.

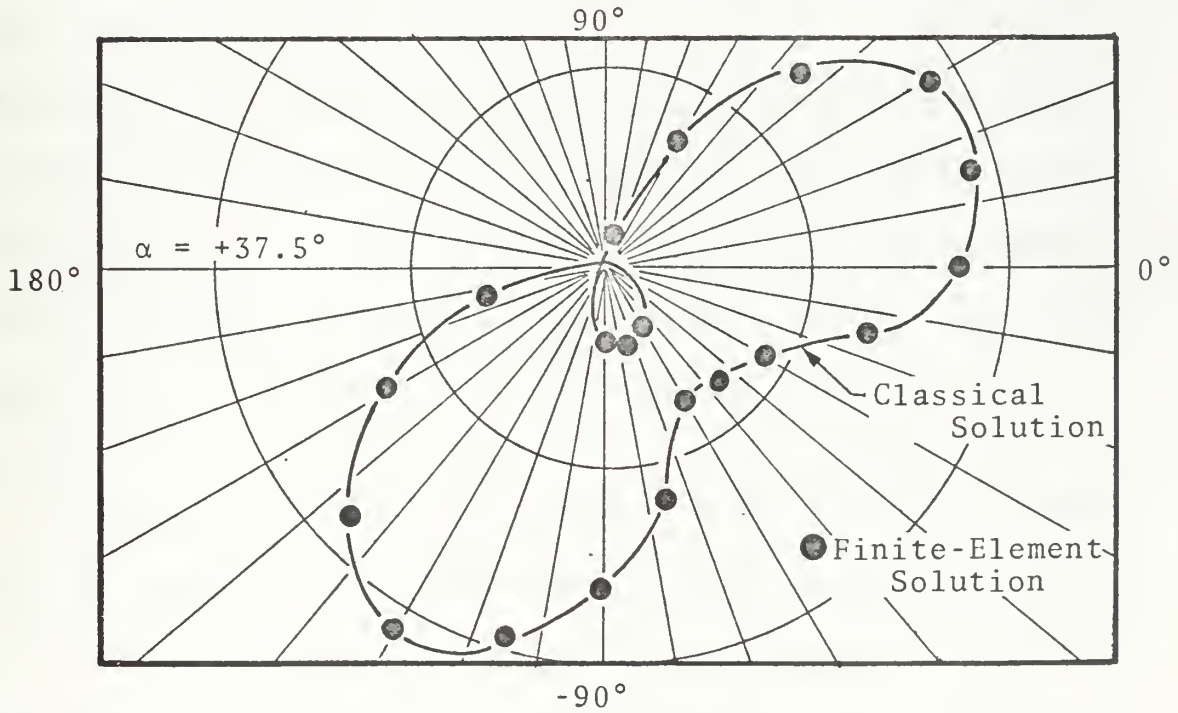

Figure 12. Typical Displacement Curves at r = Constant.

expressing the stresses or displacements at two points within the field. In the region of classical behavior, the values obtained should be independent of the points selected. Since the solution by this method is dependent upon adherence to the classical formulation, accurate results rely upon upon precise r and θ behavior.

b. Energy Release Rates

A second technique for evaluating K_I and K_{II} utilizes the energy relationships of Irwin. The work at the moving boundary is computed for two solutions under identical loading conditions, one having an incremental crack extension. Since mesh grid generation is complex and time consuming, and relocation of the nodal point coordinates for a polar grid is undesirable, a simple scheme was used to provide crack extension: the nodal point coordinates of the free ends were displaced a small amount, thereby effecting a change in crack length with minimum grid modification. This is shown schematically in Figure 13.

Because the solution is linear, and K_I and K_{II} depend only on their respective displacement components, it is sufficient to evaluate the energy release rates at the two orthogonal cases of pure opening and pure shear.

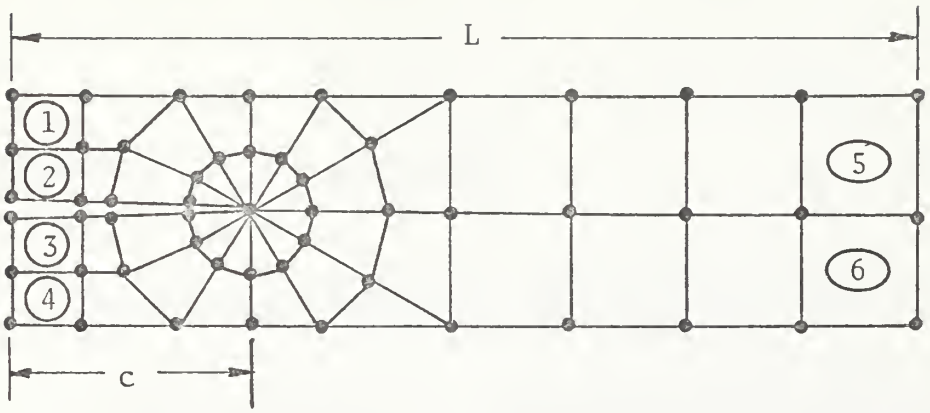

a. Original Grid Pattern.

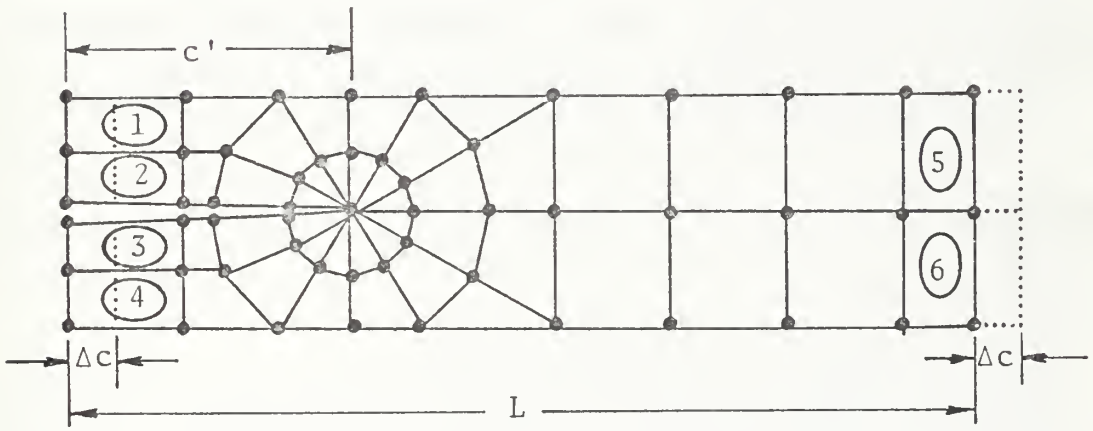

b. Extended Crack Grid Pattern
(Elements 1, 2, 3, 4 stretched; Elements 5 and 6 compressed)
(Relocate 6 Nodes at left end, 3 at right end)

Figure 13. Scheme for Extended-Crack Mesh.

This technique is preferred since it is, in effect, an "overall" or "average" solution and is not sensitive to local irregularities within the field .

c. Simplified Analysis of an Infinite Strip

A third method of evaluating K_I and K_{II} employs the simplified analysis of the infinite strip as developed by Lindsey [5]. His solution assumes that a semi-infinite crack is inserted in an infinite strip and the upper and lower boundary stresses decay to zero at some finite distance to the left of the crack tip as shown in Figure 14.

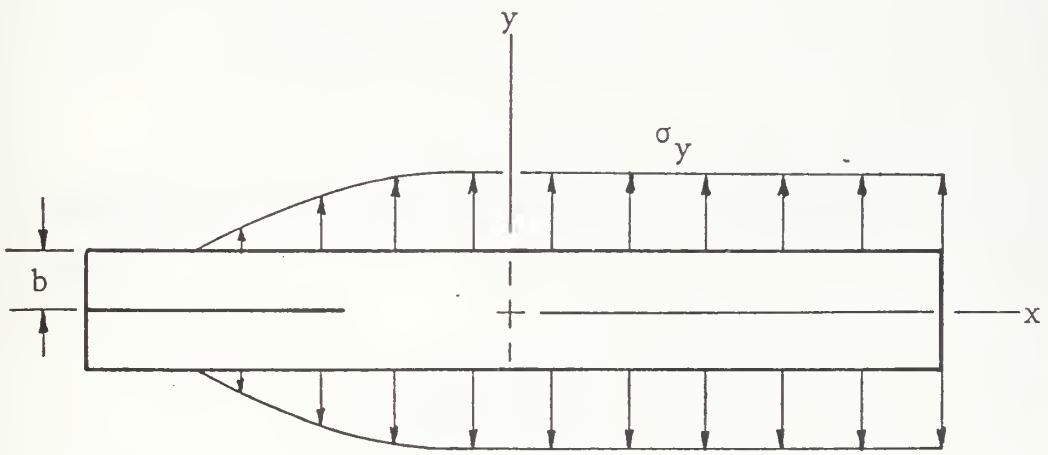

Figure 14. Infinite Strip with a Semi-infinite Crack.

"To the far left, the sheet is completely unloaded and stress free. To the far right it is under constant stress as if there were no crack,

and in the center there is a transition region of unknown character between the two constant fields. If the crack advances by an amount Δc, the transition region moves ahead Δc. The constant stress field is reduced in dimension by Δc and the unstressed region is increased by the same amount. The strain energy lost from the constant stress field by the crack moving ahead Δc is

$$\Delta U = \tfrac{1}{2}\sigma_y \varepsilon_y \cdot 2bt\Delta c \tag{10}$$

where t is the thickness of the sheet." [5]

In the limit of infinitesimal increments in crack length,

$$\frac{dU}{dc} = \sigma_y \varepsilon_y bt = \frac{\sigma^2}{E} bt \tag{11}$$

Imposing displacement boundary conditions, Lindsey shows that

$$K_I = \frac{E}{\sqrt{1-\nu^2}} \left(\frac{v_o}{b}\right) \sqrt{b} \tag{12}$$

and in a parallel development for K_{II}

$$K_{II} = \frac{E}{\sqrt{2(1+\nu)}} \left(\frac{u_o}{b}\right) \sqrt{b} \tag{13}$$

where v_o and u_o are the initial displacements. Although the geometry studied herein is far from the infinite-strip case of Lindsey, his results differ by less than two percent from the finite-element energy solution in the case of K_I.

For the parallel case of K_{II}, the agreement is not so close, the finite-element solution to K_{II} being ten percent lower than that of the infinite strip. The disagreement may be accounted for by examining the assumption of a decayed stress field to the left of the crack tip. In the opening mode, the normal boundary stress did in fact decay to zero within a short distance of the crack tip. The finite-element stress solution for this case is shown in Figure 15a. Extending the crack simply translated the gradient region and, in effect, the result was a foreshortening of the constant stress field by the amount Δc as assumed.

In the Mode II case, a boundary shear distribution of the PSELST solution is shown in Figure 15b. It can be seen that the shear stress does not decay to zero for the short geometry studied, but rather remains at a significant level

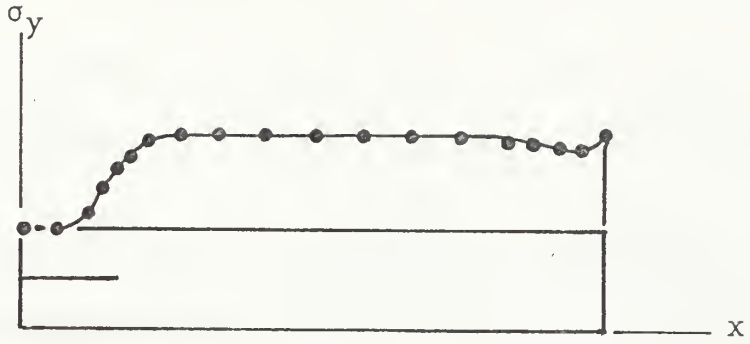

a. Normal Stress in Mode I Loading.

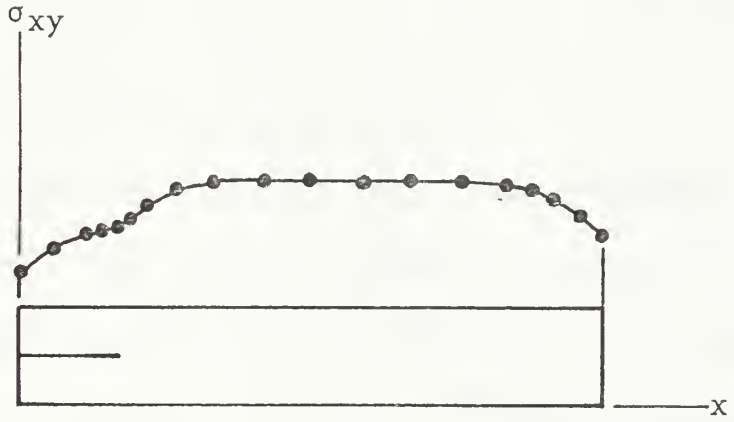

b. Shear Stress in Mode II Loading.

Figure 15. Stress Distributions on Specimen Upper Boundary.

even to the specimen's edge. Elongating the crack therefore has two effects: the uniform stress region is reduced by an amount Δc as in the case of Mode I; and, the gradient is extended by the amount Δc. Therefore, the resultant

boundary work, which equals the change of internal strain energy, may be considered as the reduction of the uniform stress over a length Δc plus that due to the redistribution of the shear gradient to the left of the uniform region.

Studies indicate, for the geometry considered herein, that this redistribution of shear stresses accounts for a ten percent reduction in the value of K_{II} from that of the simple case wherein the distribution translates but does not change.

B. DETERMINATION OF THE LOADING ANGLE

Except in the pure opening case, the resultant forces on the upper and lower specimen boundaries are not co-linear. This couple must be balanced by side loads. The finite-element solution is used to determine the magnitude of these unknown forces by establishing the distribution of the boundary stresses. From Figure 16 the relationship between the force resultant component along the direction of displacement (test data) and the orthogonal components corresponding to Mode I and Mode II can be determined as follows:

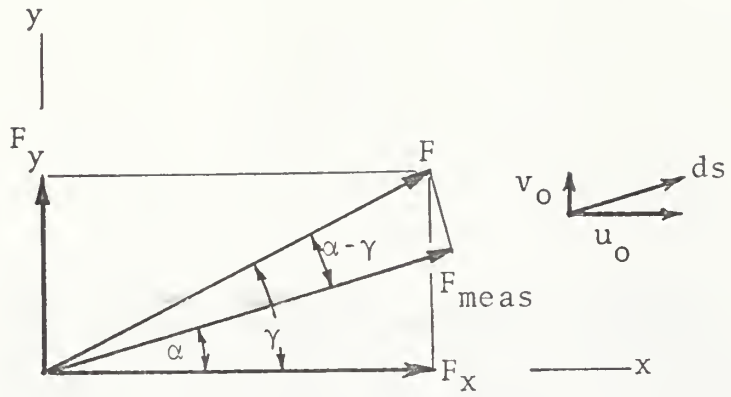

Figure 16. Diagram of Resultant Forces along Specimen Boundary.

$$F_y = F\sin\alpha = \frac{F_{meas}}{\cos(\alpha-\gamma)}\sin\alpha = C_1 F_{meas} \qquad (14a)$$

$$F_x = F\cos\alpha = \frac{F_{meas}}{\cos(\alpha-\gamma)}\cos\alpha = C_2 F_{meas} \qquad (14b)$$

If the specimen were not rigidly mounted in the fixture, the resultant force would parallel the displacement and the factors C_1 and C_2 would equal $\sin\alpha$ and $\cos\alpha$, respectively. Figure 17 illustrates the distortion of C_1 and C_2 from the preferred case of sine and cosine functions. The relationship between boundary displacement

angle and the resultant force loading angle is shown in Figure 18.

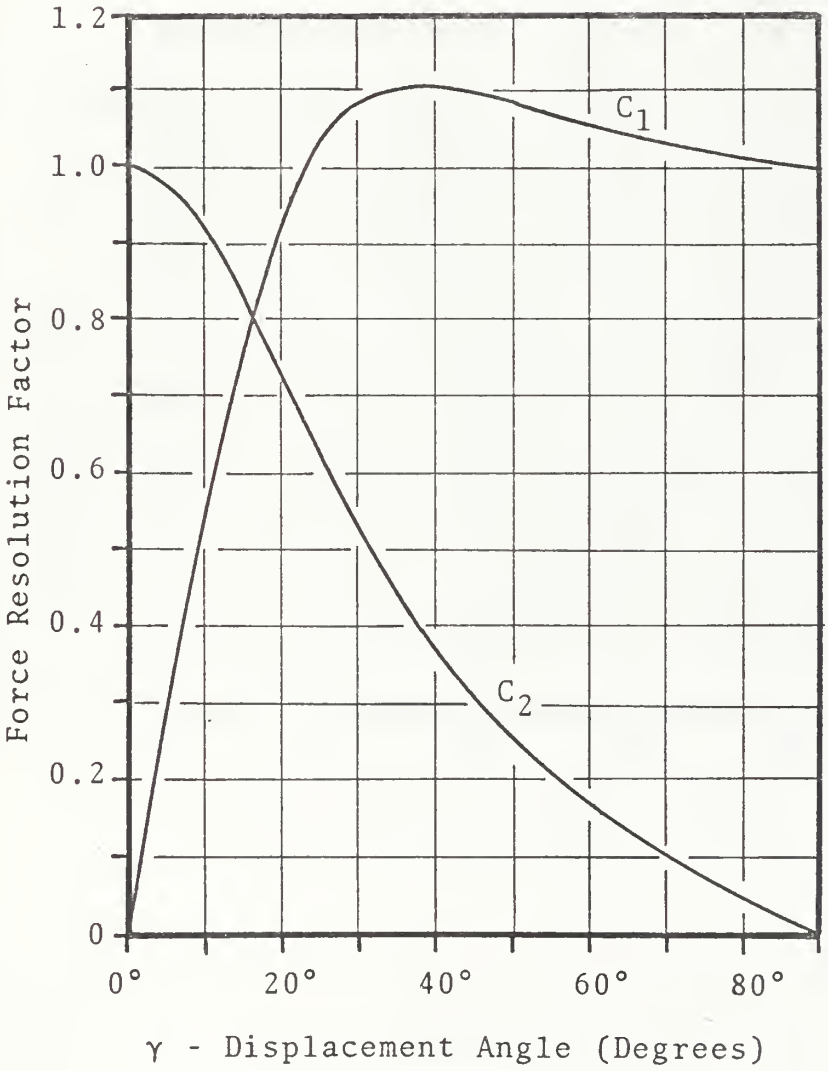

Figure 17. Force Resolution Factors.

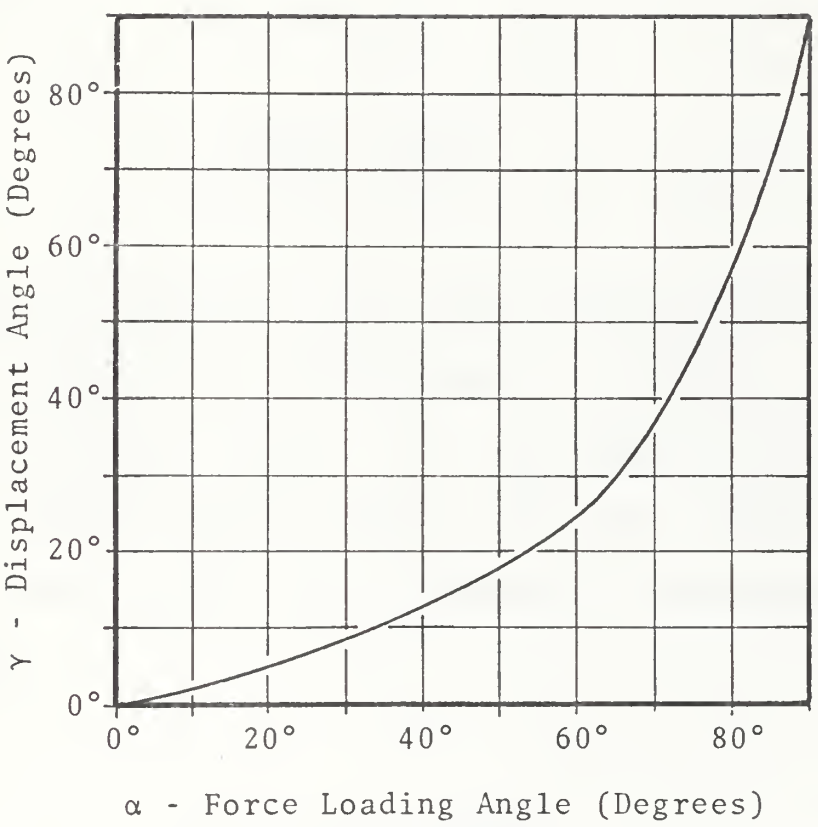

Figure 18. Displacement Loading Angle vs. Force Loading Angle.

C. EXPERIMENTAL EVALUATION OF STRESS INTENSITY FACTORS

For a linear system, the strain energy is proportional to the displacement squared. In this case it is useful to consider the separate energy components due to pure opening or pure shear in order to establish a K_I-K_{II} envelope. From Irwin we have:

$$K_I^2 = \frac{-E}{\pi t}\cdot\frac{dU}{dc} \simeq \frac{-E}{\pi t}\cdot\frac{\Delta U}{\Delta c} \tag{15}$$

A parallel analysis of the shearing mode, which assumes the crack extends an infinitesimal distance without changing direction, yields the same expression for K_{II}. Using the finite-element solution for the strain energy release rate, $\Delta U/\Delta C$, the following relationships are established:

$$K_I = 174.23\left(\frac{E}{196}\right)v_o \tag{16a}$$

$$K_{II} = 82.42\left(\frac{E}{196}\right)u_o \tag{16b}$$

where v_o and u_o are the displacements in the Mode I and Mode

II directions respectively. For the linear system, the force components are proportional to the displacements. The proportionality constants are determined by the finite-element solution. For the geometry considered, we find that:

$$u_o = \frac{F_x}{345}\left(\frac{196}{E}\right) \tag{17a}$$

$$v_o = \frac{F_y}{1244}\left(\frac{196}{E}\right) \tag{17b}$$

Equations (16) then become:

$$K_I = .1400F_y \tag{18a}$$

$$K_{II} = .2389F_x \tag{18b}$$

Using the experimental load data at fracture, the stress intensity factors of single material samples were computed and are presented in Figure 19.

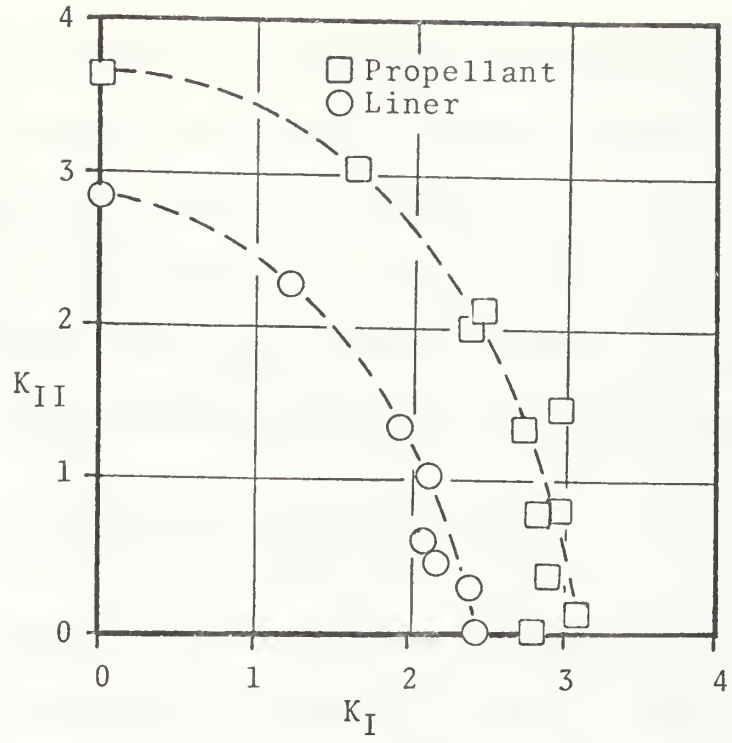

a. Single Material, Centerline Crack.

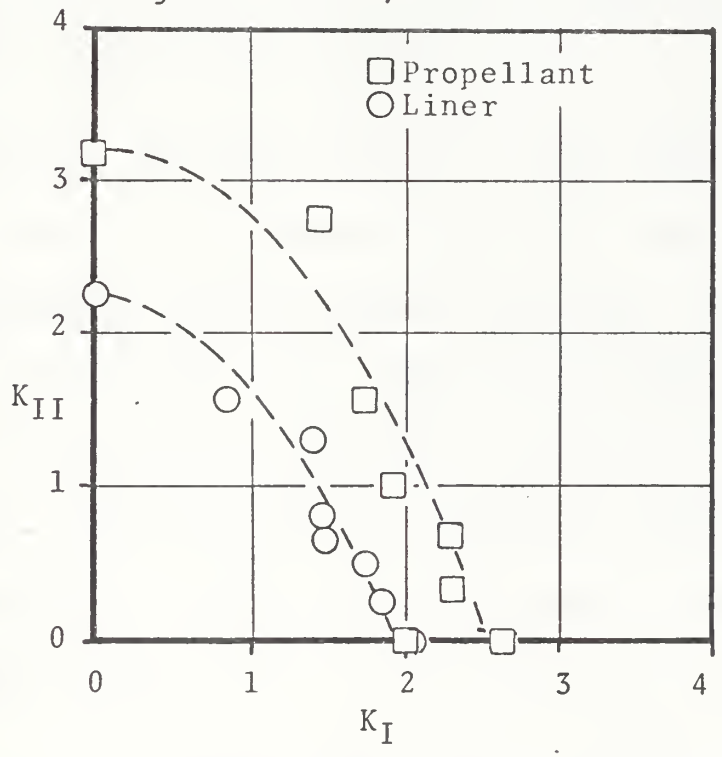

b. Single Material, Offset Crack.

Figure 19. Single-Material Fracture Envelopes.

Erdogin and Sih [6], studying the fracture of a brittle sheet (plexiglass) with oblique central cracks, found the failure envelope generally elliptic in $K_I - K_{II}$ space. However, K_{IC} (critical value of K_I where $K_{II} = 0$) was slightly larger than K_{IIC} (critical value of K_{II}), which is opposite to the viscoelastic results of this study.

D. MAXIMUM PRINCIPAL STRESS DIRECTION

Three basic techniques may be applied to determine the direction of maximum principal stress. The simplest and most obvious is to solve for the angle using the computed stress values at the crack tip nodal point.

Depending on the grid pattern, from four to twelve elements may be common to the tip node. A crack-tip-centered polar coordinate grid with 30° segments was used. Increasing the number of elements resulted in elongated elements in the vicinity of the crack tip. For a well-behaved solution, included angles of less than 30° are not recommended in order to limit the element aspect ratios to a maximum of 2:1.

On the other hand, if the polar segment angles are large and the quadrilaterals are kept low in aspect ratio, as is desired, the element size will grow too rapidly, as r

increases, to allow a sufficient number of elements in the vicinity of the crack tip for solution definition. The 30° segments used herein represent a compromise which allowed sufficient element quantity in the crack tip region while maintaining a reasonable aspect ratio. It is recognized that the solution encompassed by the inner ring of elements is questionable because of the crack tip singularity. It has been observed that even a well-conditioned element grid will not yield solution convergence within the singularity-adjacent elements.

It is interesting to note that, in spite of the solution singularity at the sharp-tipped crack node, the principal stress direction calculated from the averaged stresses at that node coincided with the test data and the blunt-tip numerical solutions. The averaged stresses were computed from the solutions of all elements common to the crack-tip node. An example is shown in Figure 20. For a boundary displacement angle of 30°, the classical sharp-tip maximum principal stress direction is 50°. The finite-element sharp-tip solution approached this value as r decreased. However, the solution diverged within two elements of the crack tip to a value of 33°, which agreed

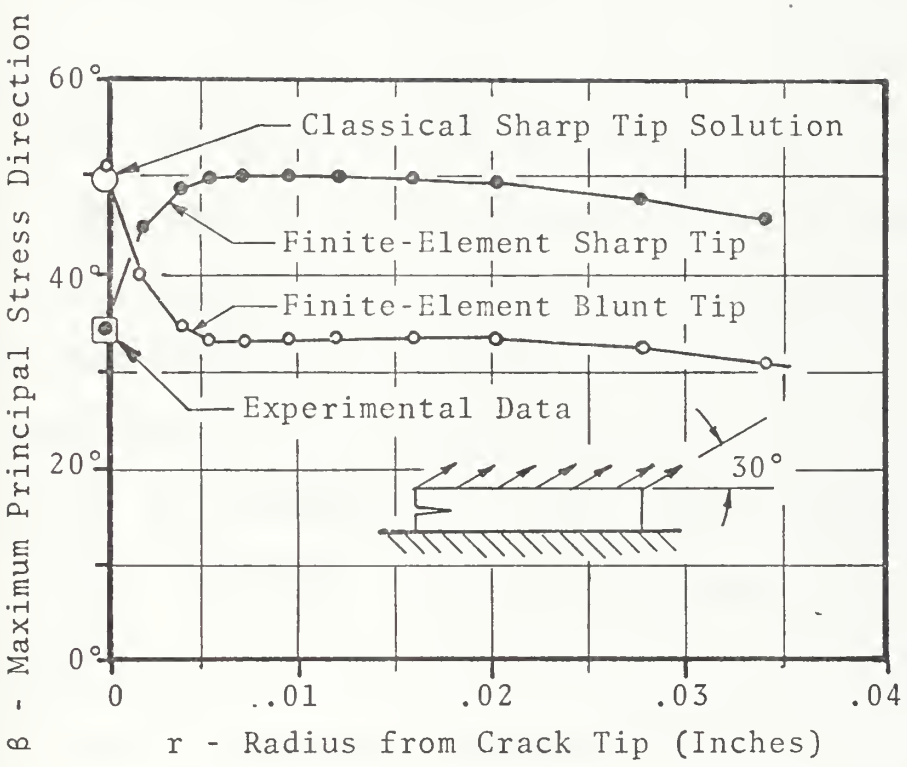

Figure 20. Comparison of Sharp and Blunt-Tip Solutions.

with the experimental trajectory for this loading. The blunt-tip solution approaches the experimental result, but it also diverged within the last element to a value of 49°. In this case, the singularity is absent and the solution divergence is typical of finite-element solutions at a free surface. At the crack tip, the finite-element solution cannot match the singularity of infinite stress. The values obtained, although fictitious, represent a solution limit in any radial direction as r approaches zero. It is quite possible that the average of these may be considered a "smearing" of the solution in the vicinity of the crack tip and that the direction of maximum principal stress can be calculated from these average stresses. This result was observed to be independent of the grid pattern. Time limitations precluded further investigation of this curiosity.

A second technique to determine the maximum principal stress direction utilizes the finite-element solution in the crack-tip near-field, excluding the singularity region. Once the limits of classical theory behavior have been established, the field within this region may be examined at fixed radius to determine the maximum stress location and its corresponding direction. If, in fact, the solution is

classically well-behaved, the angular location of the maximum stress elements should be constant although the stress magnitude changes inversely with the square root of the radius.

Superposition of Equations (1) and (3) for the case of combined loading, yields

$$\sigma_y = f_1(r)\cdot g_1(\theta, K_I, K_{II}) \tag{19a}$$

$$\sigma_x = f_2(r)\cdot g_2(\theta, K_I, K_{II}) \tag{19b}$$

$$\sigma_{xy} = f_3(r)\cdot g_3(\theta, K_I, K_{II}) \tag{19c}$$

where orientation of the element is shown in Figure 21.

For the principal stress direction:

$$\delta = \tfrac{1}{2}\arctan\left\{\frac{2\sigma_{xy}}{\sigma_x - \sigma_y}\right\} = \tfrac{1}{2}\arctan\left\{\frac{2f_3\cdot g_3}{f_2\cdot g_2 - f_1\cdot g_1}\right\} \tag{20}$$

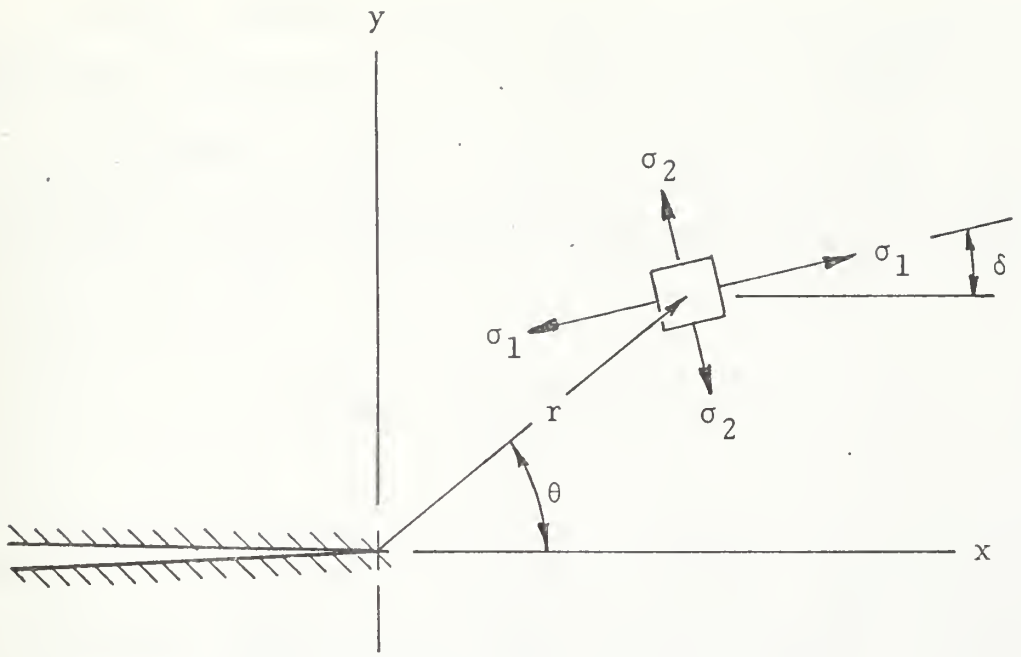

Figure 21. Principle Stress Orientation Near Crack Tip.

Since $f_1(r) = f_2(r) = f_3(r)$,

$$\delta = \tfrac{1}{2}\arctan\left\{\frac{2g_3(\theta,K_I,K_{II})}{g_2(\theta,K_I,K_{II})-g_1(\theta,K_I,K_{II})}\right\} \qquad (21)$$

which is invariant with respect to radius. The orientation is unchanging along any radius, the maximum stress having been determined at some distance from the crack tip. In the limit as r approaches zero, even though the finite-element solution diverges at the singularity, one may interpret this orientation as being the maximum principal stress at the crack tip and hence predict the trajectory for a propagating sharp-tipped crack.

A third method involves an analytical solution to Williams' equations. In the direction of maximum principal stress, the shear stress is zero. From Equation (7c) we then have, in the direction of maximum principle stress,

$$K_I \sin\beta + K_{II}(3\cos\beta - 1) = 0 \qquad (22)$$

where β is the predicted trajectory angle. Solution of this is dependent only on the ratio of K_I to K_{II} which was experimentally determined by fracture testing. The angle β corresponds to the sharp-tipped crack solution.

E. EFFECTS OF CRACK TIP RADIUS

Because of the large strain levels, the geometry of the originally sharp-tipped cracks had deformed sufficiently to approximate an elliptic shape at fracture. Figure 22 shows a typical sample wherein the propagating crack-tip geometric deformation can be seen.

The character of the crack-tip solution is dependent upon its relative bluntness. Since the crack tip radii of curvature became significant at fracture, the finite-element solution was adjusted accordingly to model this effect. It was determined that the direction of maximum principal

stress (predicted trajectory direction) was relatively insensitive to tip radius within a range of 0.004 to 0.100 inch. (The minimum radius examined was 0.004 incn). Figure 23 illustrates the sensitivity of predicted trajectory angle to crack tip radius for three selected load combinations.

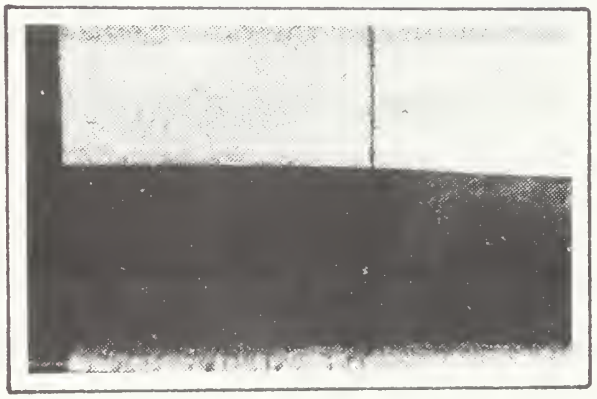

Figure 22. Crack-Tip Deformation at Fracture Loads.

Examination of the liner samples during fracture indicated tip radii in the order of 0.006 to 0.010 inch. Since the finite element solutions demonstrated trajectory insensitivity within this span of radii, the experimental results were compared with the blunt-tipped crack solutions.

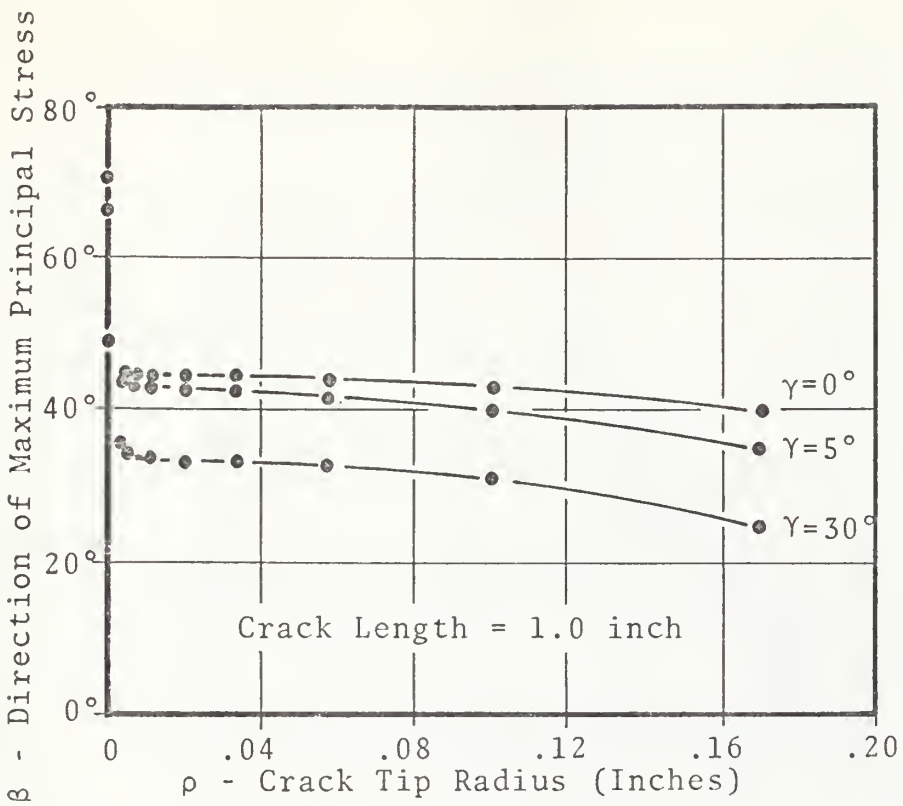

Figure 23. Effect of Crack-Tip Radius on Trajectory.

The results of single-material samples, which show excellent correlation, are presented in Figures 24 and 25.

Growth of the tip radius was not observed in the propellant samples during the fracture tests due to the erratic nature of the crack propagation. Unlike the liner, the propellant fracture tip would "stretch" and then suddenly elongate a small distance in an interrupted sequence. The resultant trajectories, however, were identical to those of the liner under similar loadings, and indicate that an effective blunting of the crack tip may have occurred.

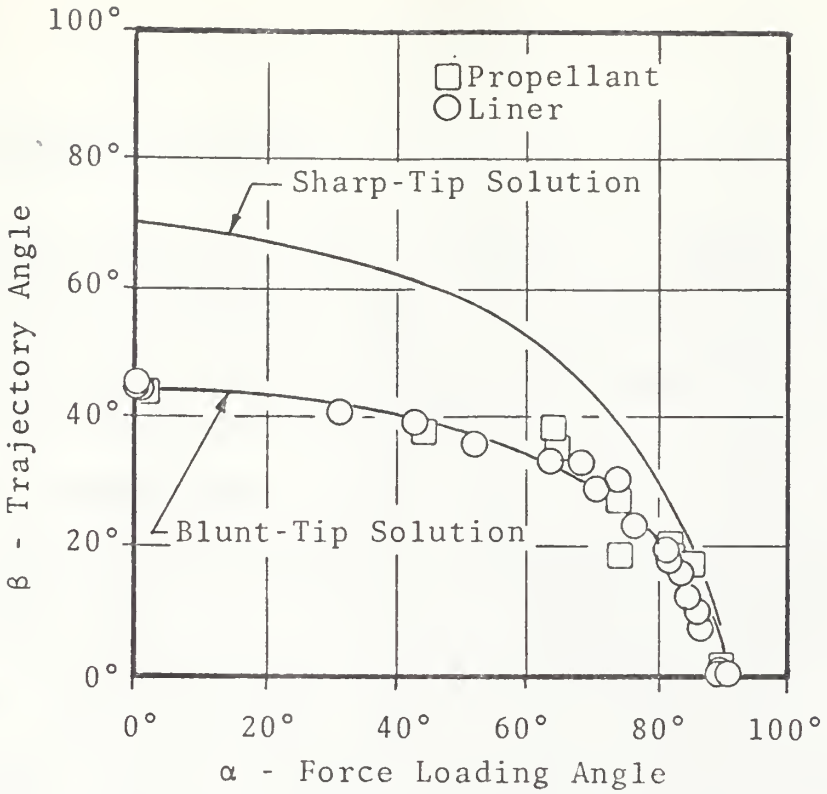

Figure 24. Single-Material, Centerline Crack Trajectories.

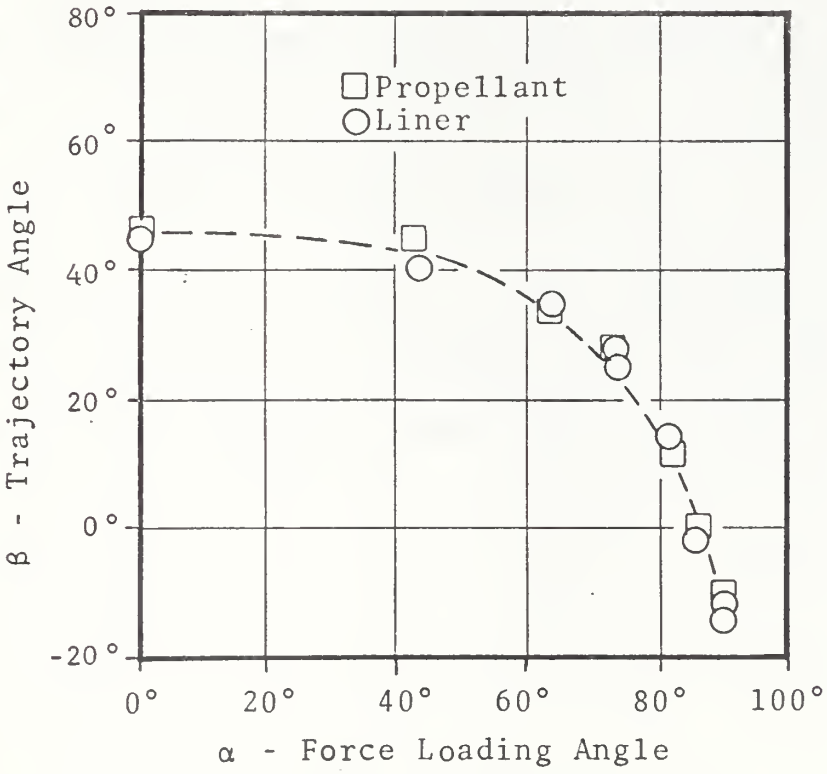

Figure 25. Single-Material, Offset-Crack Trajectories.

F. BI-MATERIAL RESULTS

Combined loading of the bi-material samples produced the fracture envelopes shown in Figures 26 and 27. The fracture trajectories are presented in Figures 28 and 29.

The propagating cracks did not, under any load orientation, continue across the liner-propellant interface. Trajectories that ran to the interface abruptly changed direction and continued along the interface. Cracks originating at the interface, or having progressed to it, would not depart from the interface regardless of loading. Post-test examination of the samples revealed that the interface cracks propagated within the propellant; that is, propellant was observed on both sides of the fracture surface. An example is shown in Figure 30.

Solution discontinuities at the interface region of bi-material finite-element studies were not sufficiently resolved to allow trajectory prediction for these samples.

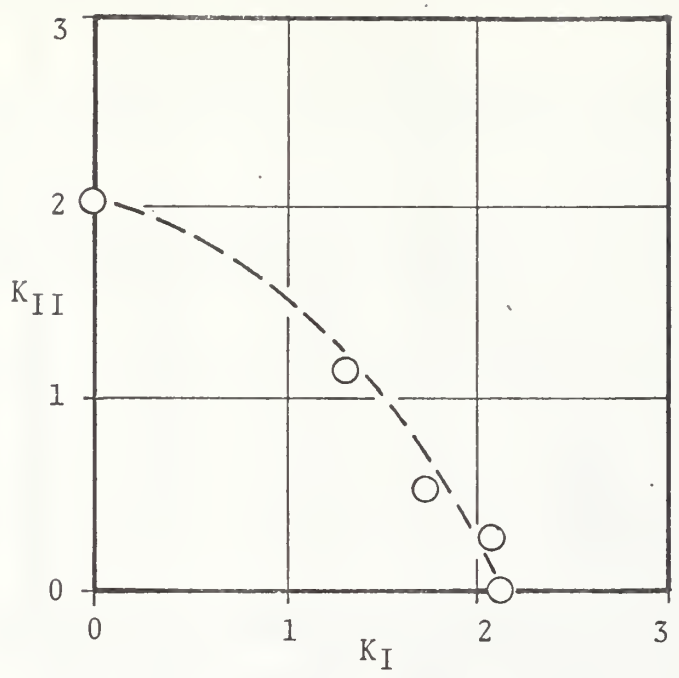

Figure 26. Bi-Material, Centerline-Crack Fracture Envelope.

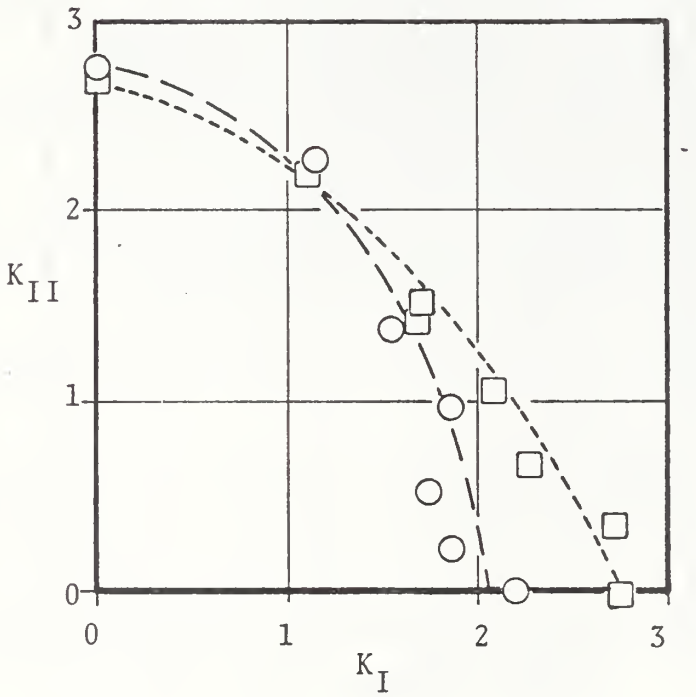

Figure 27. Bi-Material, Offset-Crack Fracture Envelopes.

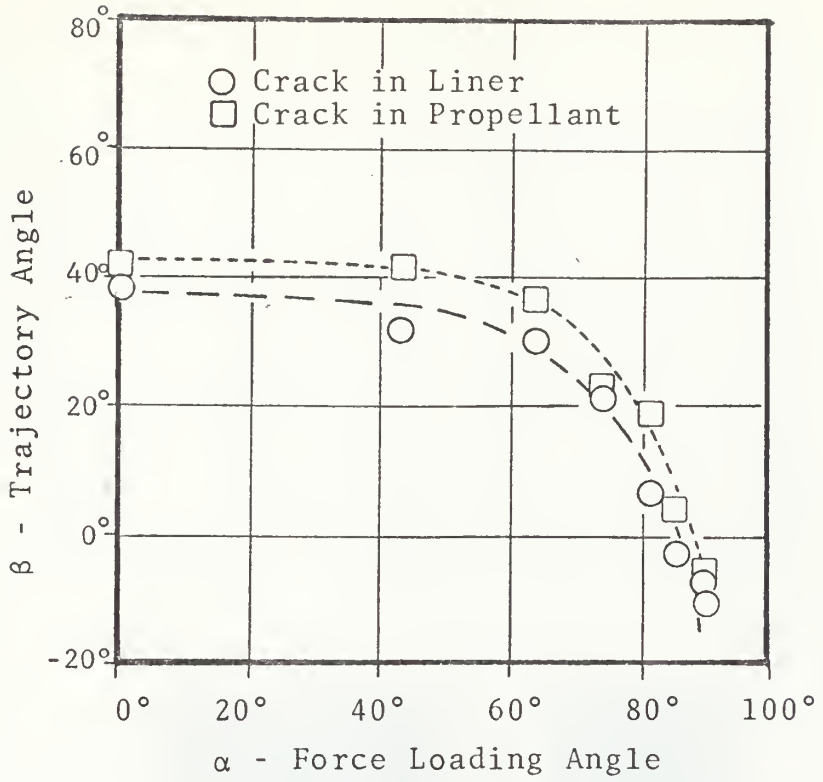

Figure 28. Bi-Material, Offset-crack Trajectories.

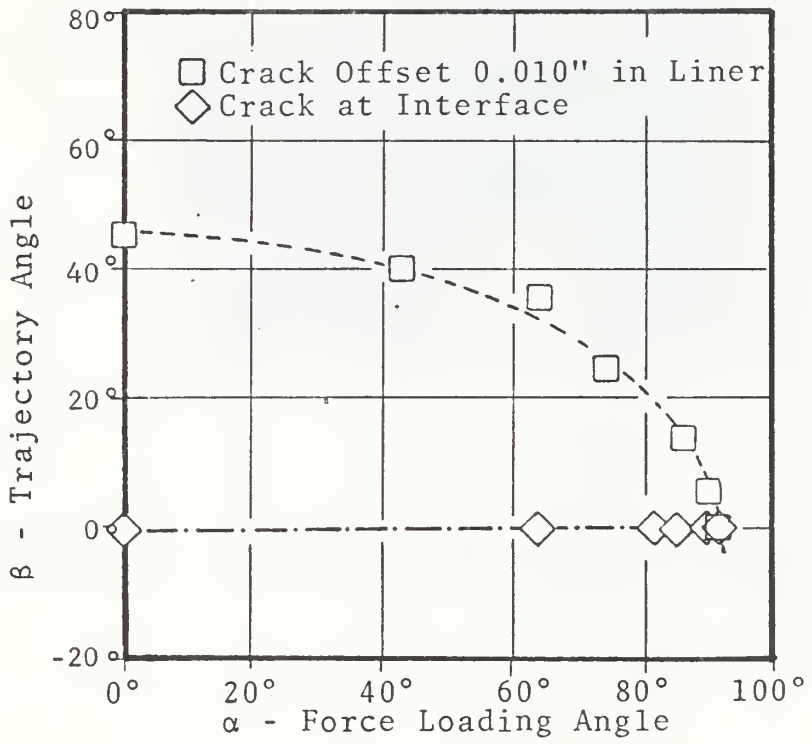

Figure 29. Bi-Material, Centerline-Crack Trajectories.

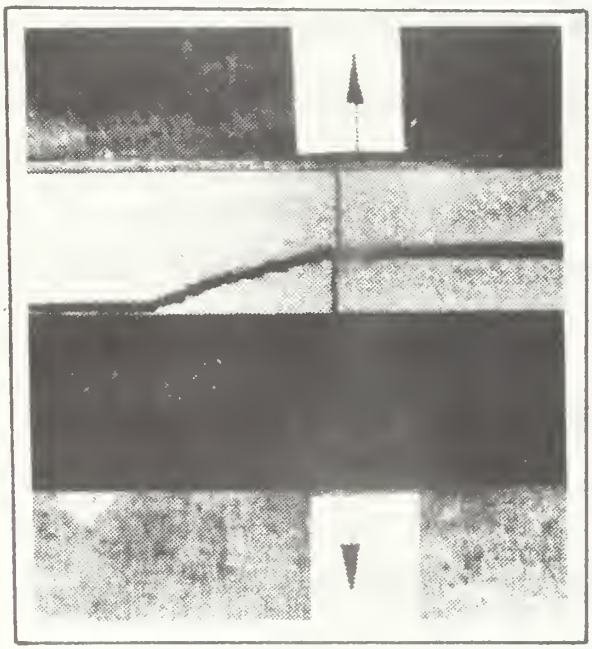

Figure 30. Photograph of Bi-Material Fracture.

V. CONCLUSIONS

The application of PSELST to crack tip analyses has been shcwn to be a highly effective solution technique for single material structures. Although the stress field cannot match the classical theory at the singularity point, the solution converges rapidly and agreement with the classical solution occurs within one or two elements from the crack tip. In addition, solution of the stress field by this program establishes the range within which classical behavior may be expected.

Because of the solution technique, the stress discontinuity at bi-material interfaces limits the effectiveness of PSELST for stress analyses in the immediate vicinity of the interface.

It has been shown that viscoelastic trajectories may be predicted using linearized analyses of elastic materials to determine the direction of maximum principal stress. In the vicinity of the crack tip, the direction of maximum principal stress is invariant with respect to radius and, in the case cf single materials, independent of the elastic modulus.

The large deformations associated with viscoelastic fracture result in an actual or effective "blunting" of the crack tip. Corresponding analyses must account for this finite radius since the stress field does not coincide with the sharp-tip solution. It has been found that the direction of maximum principal stress is invariant with tip radius within a range of 0.004 to 0.010 inch for a 1.0-inch crack length.

VI. RECOMMENDATIONS FOR FURTHER STUDY

Several areas of related interest have been identified during this study as having potential consideration for further investigation. Those which may complement this and subsequent investigations include:

A refinement of the viscoelastic sample fabrication process to eliminate the "soft" regions of incomplete cure. Uniform samples would enhance identification of the material properties, since strain data could easily be acquired simultaneously with the force data during fracture tests.

Sample testing should be performed in a limited time span, with environmental control during storage to minimize the aging and absorption of moisture, which greatly affect the material modulii.

The resultant critical loads should be studied to determine compliance (if any) with the known fracture theories.

The test fixture, which was rigidly mounted to the test machine, should be redesigned to incorporate a "floating" attachment which cannot transmit moments, thereby causing the resultant force to parallel the displacement and hence equal the measured force.

The angular range of combined loadings should be expanded. This study ranged from displacement loading angles of 0° to 90° but further studies should include the entire range of 360° if possible.

The combined load tests should be evaluated with an elastic sample of known material properties. This would allow a rapid and accurate evaluation of the test procedures and analyses.

The agreement between the blunt-tipped crack trajectory angles and the sharp-tipped solutions, determined by averaging the stresses at the tip from all elements common to it, warrants further study.

An expanded analysis should be performed to investigate the effects of large displacements in the vicinity of the crack tip.

The finite-element program should be modified to include special elements, such as long thin elements and crack-tip elements, to enhance fracture study.

The refinement of technique to minimize solution discontinuities at interfaces of different materials should be studied.

A finite-element analysis of the offset crack samples with a finite radius crack tip should be conducted to complement this study.

REFERENCES

1. G. C. Sih and H. Liebowitz, "Mathematical Theories of Brittle Fracture" in Fracture, An Advanced Treatise, p. 96, Academic Press, 1968.

2. Chemical Propulsion Information Agency Publication 214, Handbook for the Engineering Structural Analysis of Solid Propellants, by J. E. Fitzgerald and W. L. Hufferd, p. C.44, May 1971.

3. C. A. Felippa, "Refined Finite Element Analysis of Linear and Non-Linear Two-Dimensional Structures," SEL Report No. 66-22, University of California, Berkeley, 1966.

4. J. P. Malone, A Computer Program for the Analysis of Linearly Elastic Plane-Stress, Plane-Strain Problems, M. S. Thesis, Naval Postgraduate School, Monterey, California, 1968.

5. Naval Postgraduate School - 57Li72011A, Studies Pertaining to Solid Propellant Fracture, by G. H. Lindsey, pp. 63-68, 31 January 1972.

6. F. Erdogan and G. C. Sih, "On the Crack Extension in Plates Under Plane Loading and Transverse Shear," Transactions of the ASME Journal of Basic Engineering, p. 519, December 1963.

INITIAL DISTRIBUTION LIST

		No. Copies
1.	Defense Documentation Center Cameron Station Alexandria, Virginia 22314	2
2.	Library, Code 0212 Naval Postgraduate School Monterey, California 93940	2
3.	Professor G. H. Lindsey, Code 57Li Department of Aeronautics Naval Postgraduate School Monterey, California 93940	1
4.	Professor G. Cantin, Code 59Ci Department of Mechanical Engineering Naval Postgraduate School Monterey, California 93940	1
5.	Chairman, Code 57 Department of Aeronautics Naval Postgraduate School Monterey, California 93940	1
6.	LT Stephen A. Marinshaw, USN Projects Office Naval Air Rework Facility Pensacola, Florida 32508	1
7.	Mr. E. C. Francis United Technology Center P. O. Box 358 Sunnyvale, California 94088	1

Security Classification

DOCUMENT CONTROL DATA - R & D

(Security classification of title, body of abstract and indexing annotation must be entered when the overall report is classified)

ORIGINATING ACTIVITY (Corporate author)

Naval Postgraduate School
Monterey, California 93940

2a. REPORT SECURITY CLASSIFICATION

Unclassified

2b. GROUP

REPORT TITLE

Combined Loading Fracture Trajectories of Viscoelastic Materials

DESCRIPTIVE NOTES (Type of report and, inclusive dates)

Engineer's Thesis June 1973

AUTHOR(S) (First name, middle initial, last name)

Stephen Alfred Marinshaw, Jr.

REPORT DATE	7a. TOTAL NO. OF PAGES	7b. NO. OF REFS
June 1973	69	6

8. CONTRACT OR GRANT NO.	9a. ORIGINATOR'S REPORT NUMBER(S)
b. PROJECT NO.	
c.	9b. OTHER REPORT NO(S) (Any other numbers that may be assigned this report)
d.	

10. DISTRIBUTION STATEMENT

Approved for public release; distribution unlimited.

11. SUPPLEMENTARY NOTES	12. SPONSORING MILITARY ACTIVITY
	Naval Postgraduate School Monterey, California 93940

13. ABSTRACT

The critical stress intensity factors and fracture trajectories for both filled and unfilled viscoelastic plane stress specimens were experimentally determined by controlled crack elongation. Fracture testing included combined displacement loadings both of single and bi-material specimens with initial cracks located in each material and at the bi-material interface.

The feasibility of trajectory prediction using an elastic linear-strain finite-element analysis was investigated. Techniques for adapting the elastic model grid patterns to predict viscoelastic trajectories were developed.

Measured trajectories correlated well with the directions of maximum principal stress as determined by the finite-element solution of a blunt crack-tip model.

D FORM 1 NOV 68 1473 (PAGE 1)

S/N 0101-807-6811

Security Classification

A-31408

KEY WORDS	LINK A		LINK B		LINK C	
	ROLE	WT	ROLE	WT	ROLE	WT
Crack Propagation						
Finite-Element Analysis						
Fracture						
Fracture Mechanics						
Fracture Trajectories						
Propellant Fracture						
Stress Intensity Factor						
Viscoelastic Fracture						
Viscoelastic Trajectories						

Thesis
M3427 Marinshaw
c.1
145030
Combined loading fracture trajectories of viscoelastic materials.